IEEE Photonics Journal
An IEEE Photonics Society Publication

Open Access

A Tunable Polarization Beam Splitter Based on Magnetic Fluids-Filled Dual-Core Photonic Crystal Fiber

Volume 9, Number 1, February 2017

Jianshuai Wang
Li Pei
Sijun Weng
Liangying Wu
Lin Huang
Tigang Ning
Jing Li

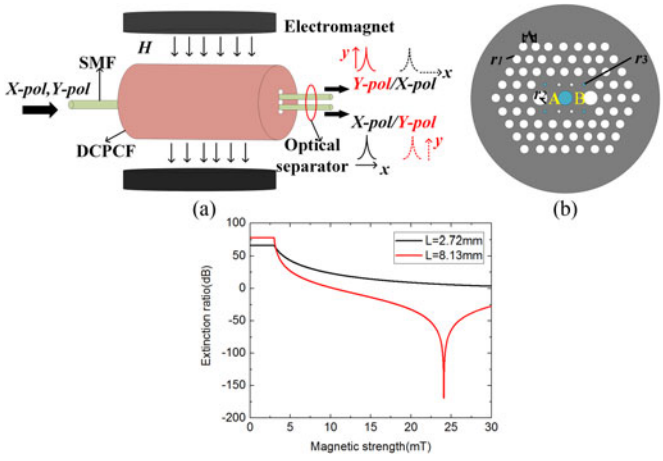

DOI: 10.1109/JPHOT.2017.2656248
1943-0655

A Tunable Polarization Beam Splitter Based on Magnetic Fluids-Filled Dual-Core Photonic Crystal Fiber

Jianshuai Wang, Li Pei, Sijun Weng, Liangying Wu, Lin Huang, Tigang Ning, and Jing Li

Key Laboratory of All Optical Network and Advanced Telecommunication Network, Institute of Lightwave Technology, Beijing Jiaotong University, Beijing 100044, China

DOI:10.1109/JPHOT.2017.2656248

Manuscript received November 8, 2016; revised January 16, 2017; accepted January 18, 2017. Date of publication February 2, 2017; date of current version February 9, 2017. This work was supported by the National Natural Science Foundation of China under Grant 61525501. Corresponding author: Li Pei (e-mail: lipei@bjtu.edu.cn).

Abstract: A tunable polarization beam splitter (PBS) is proposed based on a dual-core photonic crystal fiber (DCPCF). The DCPCF is filled with magnetic fluids in the air holes, whose refractive index varies with the magnetic field strength. The two polarized modes are separated into the two cores at the output ports in a magnetic-free condition. When magnetic field is applied, the output intensities of the two polarized modes would fluctuate. The polarized modes can be ported out with arbitrary proportion by adjusting the magnetic field intensity. Moreover, the polarized mode would be completely converted at some magnetic field strength. The properties of the DCPCF are investigated by the finite element method (FEM), including mode-conversion magnetic field strength, extinction ratio, fabrication tolerance of the PBS, and the performance of PBS at various temperatures. The numerical results show that at 1550-nm wavelength, the length of the tunable PBS is 8.13 mm. The polarized mode converts at a magnetic intensity of 25 mT with a high extinction ratio greater than −100 dB. In addition, the tunable PBS sustains a fabrication tolerance of at least 0.5% and works well at temperatures in the range of 0–55 °C by adjusting the magnetic field strength.

Index Terms: Polarization beam splitter, dual-core photonic crystal fiber, magnetic fluids, mode-conversion magnetic strength.

1. Introduction

The polarization beam splitter (PBS) is a device that can split one light beam into two orthogonal polarization states. PBS is widely used in optical communication systems, fiber-optic sensors, electro-optic detectors, etc. Over the years, many types of PBSs have been reported that have utilized various designs. Su *et al.* have demonstrated an integrated four-port polarizing beam splitter. The device operated on the principle of mode evolution and was implemented in a silicon-on-insulator platform [1]. *Kim et al.* have designed and demonstrated a polarization beam splitter based on a bridged directional coupler composed of silicon photonic devices [2]. PBSs based on silicon photonic devices are compact and show good properties [3], but most of them have relatively complex structures and fabrication limitations. Due to that, interest has emerged in the components in glass waveguides and optical fibers. The PBSs based on glass directional couplers are reported,

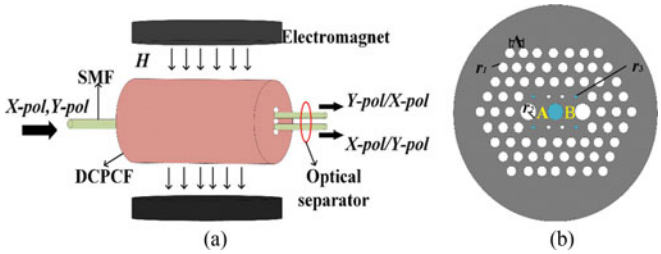

Fig. 1. (a) Schematic of the tunable PBS based on DCPCF, where X and Y polarized modes are ported in DCPCF at input side, and X and Y polarized modes are separated at the output port. (b) Cross section of the proposed DCPCF.

in which the two polarization states have different coupling lengths and are almost completely coupled to two different channels after a certain distance. However, the birefringence from glass material is usually small, which leads to a long splitter length [4]. Photonic crystal fibers (PCFs) are promising candidates for PBSs because of its natural high birefringence. For PBSs, mounts of structures based on PCFs have been designed and have included dual-core PCFs (DCPCF) [5]–[10] and three-core PCFs (TCPCF) [11]. PBSs based on DCPCF and TCPCF are mostly analyzed by the couple mode theory. Through couple mode theory, the two polarization lights are separated into two cores at output side for a certain transmission distance. Recently, PBS based on metal-filled DCPCFs have been researched [5], which are of high extinction ratios and short length. The metallic PBS works based on surface plasmon resonance (SPR) effect. Because of the SPR effect, the transmission mode would be coupled with the surface plasmon mode at some wavelength, which improves the properties of the PBS. Nevertheless, a tunable PBS has been hardly analyzed.

Magnetic fluid (MF) is such a kind of nanoparticle magneto optical material which exhibits both the magnetism like solid material and fluidity like liquid material. Under external magnetic field, the nanoparticles form chains along the magnetic field direction and the MF exhibits magneto-optical effects, such as birefringence, Faraday effect, transmission, etc. The refractive index (RI) of the magnetic fluids (n_{MF}) can be tuned by adjusting the external magnetic field strength [12]–[14]. Based on the properties of MF, researches have been demonstrated for magnetic controllable wavelength-division multiplexers (WDM) [15], magnetic field sensing [16], magnetic modulators [17], etc.

In this paper, we proposed a tunable polarization beam splitter based on MF-filled DCPCF. The output polarized light is tunable by adjusting the strength of magnetic field. For one core, only Y-polarized mode is obtained in a free magnetic field. When an external magnetic field applied, the effective RI (n_{eff}) of the propagation modes will be changed due to the RI variation of the MF. Consequently, the coupling length of the two polarized modes would be as a function of the magnetic field strength. As a result, Y-polarized mode will be replaced by X-polarized mode at a certain magnetic field strength. The finite element method (FEM) is applied by investigating the characteristics of the device including, mode-conversion magnetic strength, extinction ratio, device size and the fabrication tolerance of the PBS. At 1550 nm wavelength, the simulation results show that the device can achieve polarized mode conversion at the length of 8.13 mm. The mode-conversion magnetic strengths is 25 mT with an extinction ratio higher than -100 dB. In addition, the PBS has a good structural flexibility and works well in the range of temperature 0–55 °C by adjusting the magnetic field strength.

2. Structure and Theoretical Modelling

The schematic of the tunable PBS is illustrated in Fig. 1(a). A light, X and Y-polarized beam, is ported in DCPCF at the input side with a pieces of single-mode fiber (SMF). At the output side, the two polarized lights are separated into the two cores by an optical separator. The overall configuration is placed amid a uniform magnetic field which is supplied by an electromagnet with

two poles. The magnetic strength can be adjusted by controlling the distance between the two electromagnetic poles. In a free magnetic field, the X and Y polarized lights are ported out from the two cores respectively. When a proper magneto applied, the two polarized output mode from the two cores would exchange. The cross section of the proposed PBS based on DCPCF in this paper is illustrated in Fig. 1(b), where Λ is the air-holes pitch, r_1, r_2, r_3 are the normal, extended and compressed air-holes radius, respectively. The centers of the all air-holes are situated at a hexagonal lattice. The two identical cores, *A* and *B*, are formed by removing two air-holes in each core respectively. The background material is pure silica, and its dispersion relation is calculated by the Sellmeier equation [18].

The air holes, located close to the cores (air holes in blue), are filled with MF as shown in Fig. 1(b). The MF changes from the random homogenous state to the field dependent structural pattern state when an external magnetic field is applied. The nanoparticles in the MF agglomerate and further form chains as well as magnetic columns along the direction of magnetic field. During the process of the formation of the magnetic columns, phase separation occurs between the columns and liquid in MF under the external magnetic field, which causes the variation of the effective dielectric constant of MF and, meanwhile, causes RI variation of the MF. The effective dielectric constant of MF is given in [17]. The n_{MF} does not change until the field strength exceeds a critical value, and then increases with rising field strength, reaching a saturated value under higher strengths. The RI of the MF depends on the concentration, the temperature and magnetic field strength, etc. The RI of MF is described as a function of the magnetic strength and temperature in detailed [19]:

$$n_{MF}(H, T) = (n_s - n_0)\left[\frac{\coth(\alpha(H - H_c)}{T} - \frac{T}{\alpha(H - H_c)}\right] + n_0 \,(\text{For } H > Hc) \tag{1}$$

where n_o is the RI of the MF under fields lower than *Hc* that depends on the type of carrier liquid and the concentration of MF, and n_s denotes the saturated value of the RI of the MF. *H* is the field strength in mT, *T* is the temperature in Kelvin, and α represents the fitting parameters. In this paper, a water-based MF with a particle volume concentration of 0.16 emu/g is applied, and *Hc* is assumed 3 mT. The temperature is set to be 24.3 °C. The RI of MF n_0 is 1.355 under the value of 3 mT for magnetic field strength [20].

According to the optical waveguide theory, there are four supermodes propagating in DCPCF named X-even, Y-even, X-odd, and Y-odd. For an effective PBS, the coupling characteristics can be obtained through couple mode theory. Coupling length of the polarization splitter at a given wavelength is defined by the following equation:

$$L_x = \frac{\lambda}{2(n^x_{even} - n^x_{odd})} \tag{2}$$

$$L_y = \frac{\lambda}{2(n^y_{even} - n^y_{odd})} \tag{3}$$

where $n^{x,y}_{even}$, $n^{x,y}_{odd}$ are the effective refractive index (n_{eff}) of the four supermodes and λ denotes the wavelength of the light at free space. Assuming that the light is launched into core *A* at the input side. Owing to the mode coupling in DCPCF, the light would be ported out from both cores. The normalized output powers of the two polarized lights in core *A* and core *B* are described by

$$p^x_A = \cos^2\left(\frac{\pi z}{2L_x}\right) \tag{4}$$

$$p^y_A = \cos^2\left(\frac{\pi z}{2L_y}\right) \tag{5}$$

$$p^x_B = \sin^2\left(\frac{\pi z}{2L_x}\right) \tag{6}$$

$$p^x_B = \sin^2\left(\frac{\pi z}{2L_x}\right) \tag{7}$$

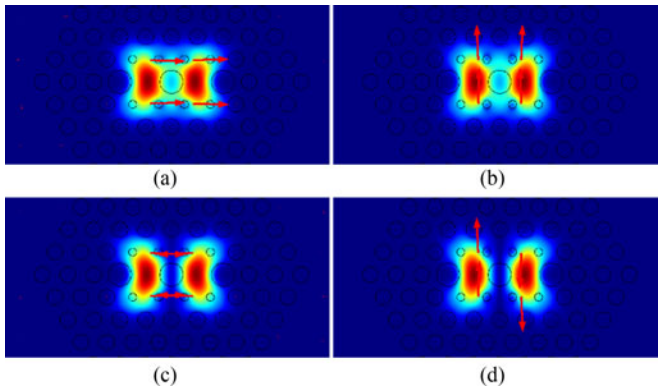

Fig. 2. Electric field distributions, at 1550 nm of (a) X-even, (b) Y-even, (c) X-odd, and (d) Y-odd mode without applying magnetic field at $r_1 = 0.6\ \mu$m, $r_2 = 0.89\ \mu$m, $r_3 = 0.3\ \mu$m, and $\Lambda = 2\ \mu$m.

where z is on behalf of the transmission distance. Due to the nonuniformity of the air holes, a high birefringence exhibits in DCPCF. Therefore, the coupling length of the two polarized modes will be different. If $mL_x = nL_y = L$ (m and n are positive integers with opposite parity, L is the length of the splitter), at the end of the splitter, light of the Y-polarized remains in core A, while light of the X-polarize is coupled into core B, i.e., and the two orthogonal polarization components of the light are separated from each other. For the two output ports, core A is analyzed only in the following and the properties of core B are on the contrary. Coupling length ratio (CLR) is defined as

$$CLR = \frac{m}{n} = \frac{L_y}{L_x}. \tag{8}$$

In order to obtain a compact PBS, the value of CLR is vital, which is analyzed in the following section. Beyond that, the extinction ratio (ER) is also an important parameter to evaluate the quality of a PBS. It is defined as the power of a particular polarized mode in the expected output core comparing to the power of the other polarized mode in the same core. As the properties of core A analyzed only, the extinction ratio is defined as follows:

$$ER = 10 \lg \frac{P_A^y}{P_A^x}. \tag{9}$$

3. Results and Analysis

There are four supermodes propagating in DCPCF named X-even, Y-even, X-odd, and Y-odd. Fig. 2 illustrates the electric field distributions of (a) X-even, (b) Y-even, (c) X-odd, and (d) Y-odd mode without applying magnetic field at 1550 nm wavelength, where $\Lambda = 2\ \mu$m, $r_1 = 0.6\ \mu$m, $r_2 = 0.89\ \mu$m, and $r_3 = 0.3\ \mu$m.

In order to obtain a compact PBS, the coupling lengths and CLR as a function of the geometric parameters are investigated in Fig. 3. The two coupling lengths varies within the range of 0.22 to 0.65 mm. As depicted in Fig. 3(a), Lx reduces corresponding to the radius of the normal air hole, while Ly barely changes simultaneously. Moreover, the coupling lengths, Lx and Ly, increase linearly with the radius of extended air hole, the radius of the compressed air hole and the pitch between air holes as shown in Fig. 3(a)–(c), respectively. CLR grows relating to the radius of the three kinds of air holes and decreases with the air hole pitch. Additionally, as shown in Fig. 3, CLR is sensitive to the radius of the compressed air hole, while insensitive to the other parameters. In order to obtain a device of small size, the CLR is set to be 1.25, where the DCPCF is characterized by the parameters $r_1 = 0.8\ \mu$m, $r_2 = 1\ \mu$m, $r_3 = 0.538\ \mu$m, and $\Lambda = 2\ \mu$m.

The normalized output optical power as a function of propagation distance at 1550 nm wavelength is illustrated in Fig. 4, where $\Lambda = 2\ \mu$m, $r_1 = 0.8\ \mu$m, $r_2 = 1\ \mu$m, and $r_3 = 0.358\ \mu$m. One can clearly

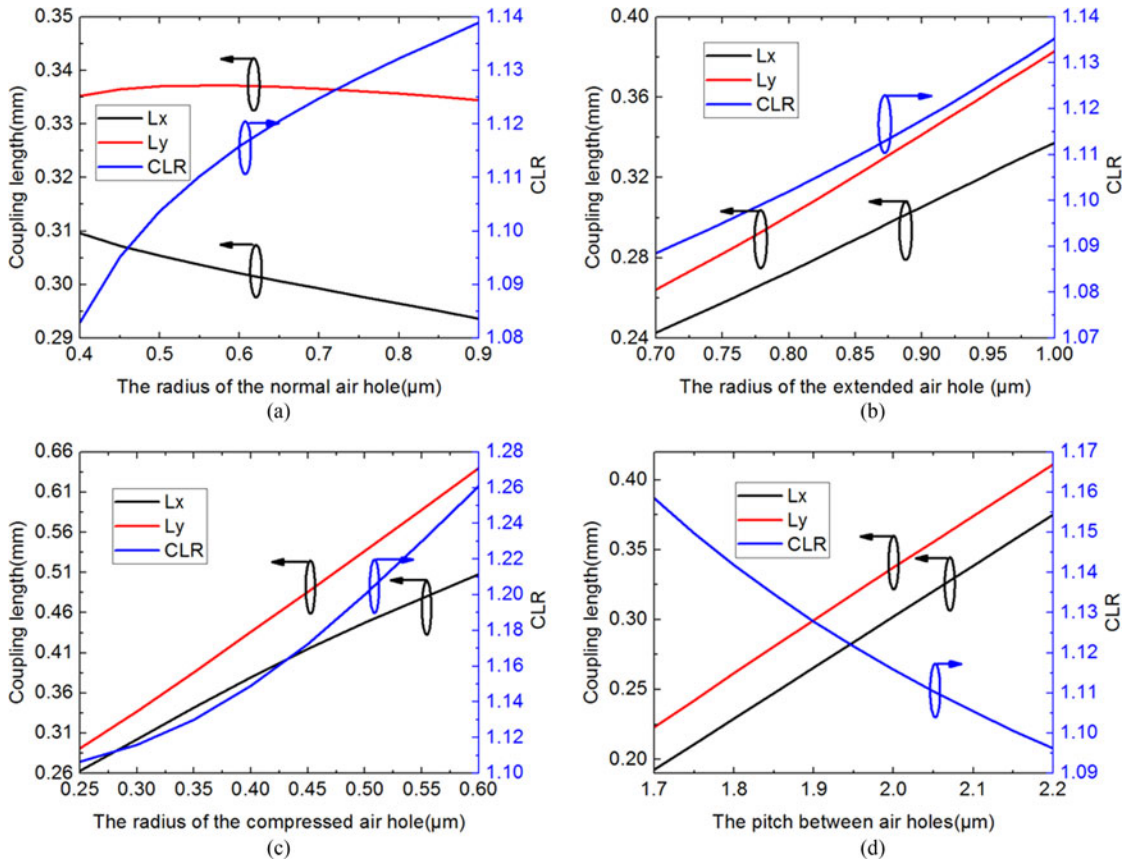

Fig. 3. Coupling lengths and CLR versus (a) radius of the normal air hole at $r_2 = 0.89\ \mu$m, $r_3 = 0.3\ \mu$m, and $\Lambda = 2\ \mu$m. (b) Radius of the extend air hole at $r_1 = 0.6\ \mu$m, $r_3 = 0.3\ \mu$m, and $\Lambda = 2\ \mu$m. (c) Radius of the compressed air hole at $r_1 = 0.6\ \mu$m, $r_2 = 0.89\ \mu$m, and $\Lambda = 2\ \mu$m. (d) Pitch between air holes at $r_1 = 0.6\ \mu$m, $r_2 = 0.89\ \mu$m, and $r_3 = 0.3\ \mu$m at 1550 nm wavelength.

see that the lights in Y direction reaches its maximum, while lights in X direction decreasing to its minimal at the separate length of 2.71 mm. It indicates that only Y-polarized light can be obtained in core *A* at the output port, while X-polarized mode is forbidden in core *A*. Hence, the designed DCPCF can be used as a polarization splitter with a length of 2.71 mm. In fact, single-polarization output would show up periodically as the transmission distance growing. By simulation, the second order of separate length is 8.13 mm. At the separate length of 2.17 and 8.13 mm, high ERs greater than 50 dB are obtained.

Without magnetic field, Y-polarized mode is obtained from core *A* for the designed length of DCPCF. Once magnetic field applied, the RI of the MF would be various with the magnetic field strength. At temperature 24.3 °C, the RI of MF as a function of the magnetic field strength is illustrated in Fig. 5. The RI remains unchanged under 3mT for the magnetic strength and then increases with *H*. The variation of the RI of MF results in the change of the n_{eff} of the four supermodes. Consequently, the coupling lengths of the two polarized modes will be changeable as a function of the magnetic strength. The coupling lengths of X and Y-polarized modes are depicted in Fig. 6 corresponding to the magnetic strength. From Fig. 6, the coupling lengths of the both polarized lights drops monotonically as the magnetic strength growing. The variation trends of the two polarized modes coupling lengths are significantly similar that they are decreased by 4.5×10^{-2} and 4.8×10^{-2} mm at $H = 30$ mT, respectively.

Owing to the variation of the coupling length, the normalized output power varies. Fig. 7 illustrates ER as a function of magnetic field strength at 2.72 and 8.13 mm. Without magneto, the extinction

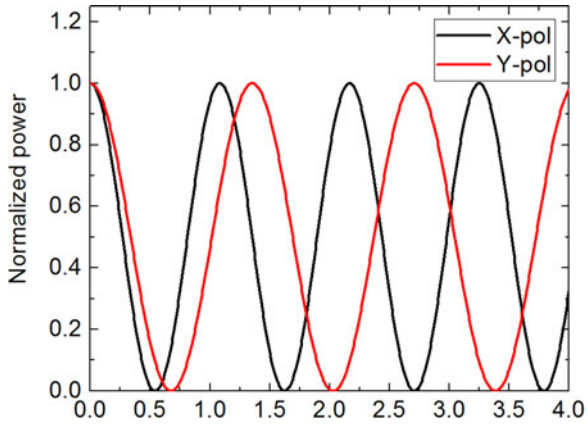

Fig. 4. Output optical power versus propagation distance without applying magnetic field at $r_1 = 0.8\ \mu$m, $r_2 = 1\ \mu$m, $r_3 = 0.538\ \mu$m, and $\Lambda = 2\ \mu$m.

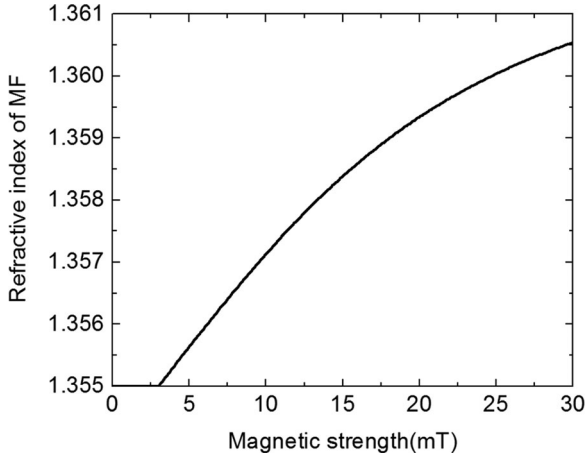

Fig. 5. Refractive index of MF versus the strength of magnetic field at temperature 24.3 °C.

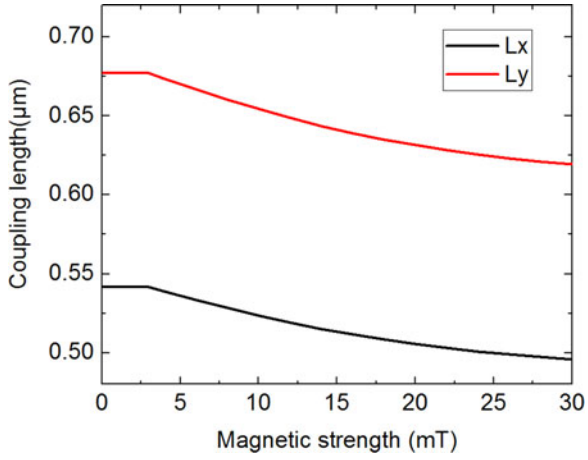

Fig. 6. Coupling length of the two polarizations versus the strength of magnetic field at $r_1 = 0.8\ \mu$m, $r_2 = 1\ \mu$m, $r_3 = 0.538\ \mu$m, and $\Lambda = 2\ \mu$m.

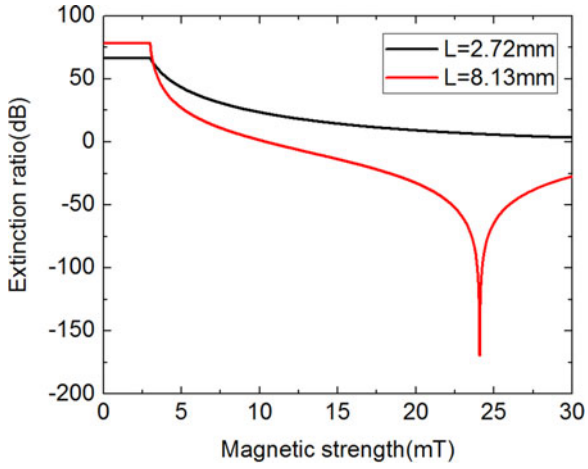

Fig. 7. ER versus the strength of magnetic field at different orders of coupling length: the first order separate length 2.72 mm and the second order separate length 8.13 mm.

ratios are greater than 60 dB for the both separate lengths, which indicates that only Y-polarized mode is received in core *A* at the output port. Because of the coupling length varying with the magnetic strength, the power of Y-polarized light reduces, as well as X-polarized light increasing inversely. Therefore, the ER decrease. For the length of 2.72 mm, the ER linearly decreases corresponding to magnetic strength, and reduces to 3 dB at $H = 30$ mT, which indicates that the polarized mode conversion cannot be achieved for the first order separate length. At $L = 8.13$ mm, the ER reduces to 0 dB with a magnetic strength of 10.3 mT, which implies the intensities of two modes are equal. Subsequently, the value of ER remains below zero, where the X-polarized exceeds the Y-polarized mode power. The ER is greater than -20 dB in the range of 17 to 30 mT. It is worth mentioning that an ultrahigh extinction ratio of -150 dB is obtained around 25 mT for the magnetic field strength. Therefore, the mode conversion can be realized with a length of 8.13 mm at $H = 25$ mT. In addition, the two polarized modes with arbitrary proportion can be obtained by adjusting the magnetic field strength for the PBS.

Due to the numerous air holes of the DCPCF, the structural accuracy may be influenced by manufacturing environment or the nonuniformity of the device itself. The fabrication flexibility is discussed as illustrated in Fig. 8. The geometrical errors are defined as Δ_i ($i = 1, 2, 3, 4, 5$), which represent the errors of the radius of normal air holes, the extended air holes, the compressed air holes, the pitch between air holes, and the length of the PBS, respectively. Without magneto, the extinction ratio are 23 dB and 21 dB for the three kinds of air holes with a structural deviation of $\pm 0.5\%$ as shown in Fig. 8(a). Moreover, at $H = 25$ mT, the extinction ratios are -27 dB and -21 dB, which indicates that the mode conversion can be also achieved regardless of the structural inaccuracy. The properties of the pitch between air holes are discussed in Fig. 8(b). In a free magnetic field, the ER are 29 and 23 dB, and at $H = 25$ mT, the ER are -31 and -21 dB for a fabrication tolerance of 0.5% and -0.5%, respectively. The tunable PBS sustains a fabrication tolerance of 0.5% for the radius of the three kinds of air holes and the distance between holes. The length accuracy is also analyzed in the Fig. 8(c). The PBS works well with a fabrication deviation of $\pm 0.75\%$, which are 8.07 and 8.19 mm, respectively. The ER are 37 dB, 32 dB at $H = 0$, and -43 dB, -29 dB at $H = 25$ mT, which means that Y-polarized mode is obtained in a free magnetic condition, and moreover, Y-polarized mode is replaced by X-polarized mode at $H = 25$ mT. The tunable PBS operates well within an error of 0.75% in length.

The RI of MF varies with the temperature according to (1). However, the RI of MF is immune to the temperature in a free magnetic field, which means n_0 is unchangeable in various temperatures. Besides, *Hc* is linearly related to the temperatures [19]. Thus, ER remains steady, resulting from the fixed n_0 without magneto. When magnetic field applied, the RI of MF changes relating to

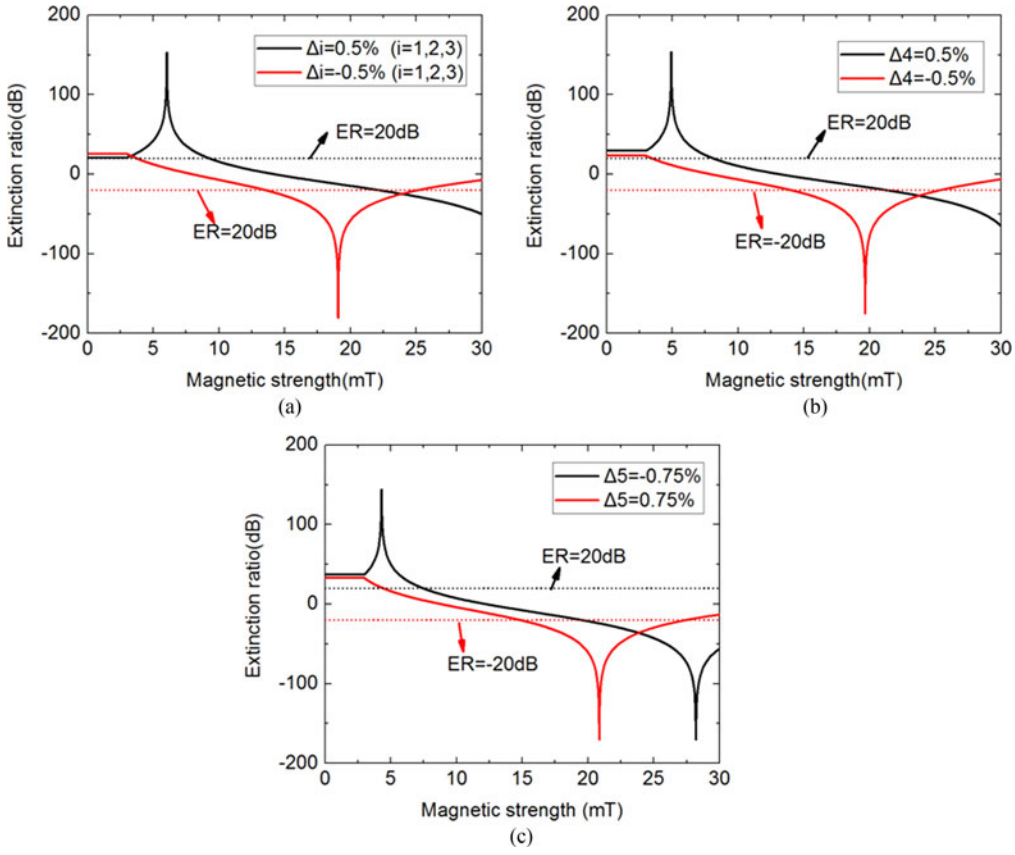

Fig. 8. ER versus the strength of magnetic field at various fabrication tolerance. (a) Three kinds of air holes with a fabrication tolerance of 0.5%. (b) Pitch between air holes with a fabrication tolerance of 0.5% at L = 8.13 mm. (c) Length of the PBS with a fabrication tolerance of 0.75% at $r_1 = 0.8$ μm, $r_2 = 1$ μm, $r_3 = 0.538$ μm, and $\Lambda = 2$ μm.

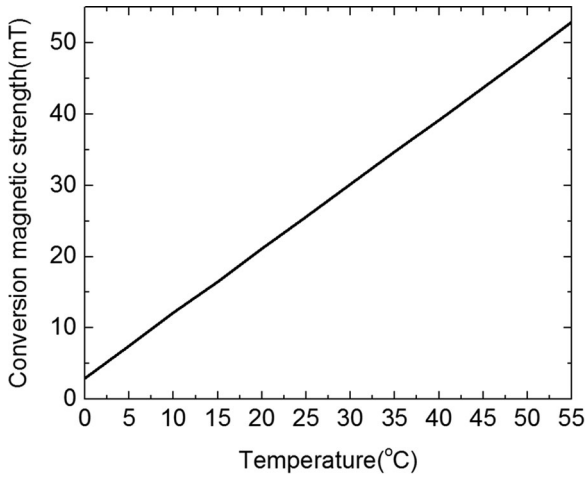

Fig. 9. Mode-conversion magnetic strength versus temperature at $r_1 = 0.8$ μm, $r_2 = 1$ μm, $r_3 = 0.538$ μm, and $\Lambda = 2$ μm.

different temperatures. Thus, the mode-conversion magnetic strength would be different at diverse conditions. The mode-conversion magnetic field strength is illustrated in Fig. 9 as a function of temperature. In the range of temperature, 0–55 °C, the mode-conversion strength has a liner relation to the temperature. At 0 °C, the magnetic strength reduces to 2.9 mT. The mode-conversion magnetic strength rises with a growing temperature and the strength increases to 52.9 mT at 55 °C. At different temperatures, the polarization modulating can be also realized by adjusting the magnetic field strength.

4. Conclusion

A tunable polarization splitter based on DCPCF is designed by filling MF into the air holes close to the two cores. The parameters of the DCPCF has been optimized for the radius of normal air holes, extended air holes, compressed air holes and the air hole pitch, which are 0.8 μm,1 μm, 0.358 μm, and 2 μm, respectively. For core *A*, only Y-polarized light can be received at the output port without magneto. By adjusting the magnetic intensity, the power of Y-polarized mode decreases, while X-polarized mode increases. Therefore, the Y-polarized mode can be replaced by X-polarized mode at some magnetic strength. At 1550 nm wavelength and a room temperature 24.3 °C, the mode-conversion magnetic strength is 25 mT. The length of the tunable PBS is 8.13 mm with a high mode-conversion extinction ratio of −150 dB. Additionally, the designed PBS has a good manufacturing flexibility. The PBS works well with a fabrication tolerance of 0.5% for the radius of the air holes and the air hole pitch. The PBS performs satisfactorily for a deviation of 60 μm form 8.13 mm in length. At various temperatures, the polarized mode conversion can be realized by adjusting the magnetic strength. The device is potential in applications to sensing, optical communication, and power modulation.

References

[1] Z. Su *et al*., "Four-port integrated polarizing beam splitter," *Opt. Lett*., vol. 39, pp. 965–968, Feb. 2014.
[2] D. W. Kim, M. H. Lee, Y. Kim, and K. H. Kim, "Planar-type polarization beam splitter based on a bridged silicon waveguide coupler," *Opt. Exp*., vol. 23, pp. 998–1004, Jan. 2015.
[3] K. W. Chang and C. C. Huang, "Ultrashort broadband polarization beam splitter based on a combined hybrid plasmonic waveguide," *Sci. Rep*., vol. 6, 2016, Art. no. 19609.
[4] G. D. Peng, T. Tjugiarto, and P. L. Chu, "Polarisation beam splitting using twin-elliptic-core optical fibres," *Electron. Lett*., vol. 26, pp. 682–683, 1990.
[5] Z. Fan, S. Li, Q. Liu, H. Chen, and X. Wang, "Plasmonic broadband polarization splitter based on dual-core photonic crystal fiber with elliptical metallic nanowires," *Plasmonics*, vol. 11, pp. 1565–1572, 2016.
[6] L. Zhang and C. Yang, "Polarization splitter based on photonic crystal fibers," *Opt. Exp*., vol. 11, pp. 1015–1020, 2003.
[7] Z. Lin and Y. Changxi, "A novel polarization splitter based on the photonic crystal fiber with nonidentical dual cores," *IEEE Photon. Technol. Lett*., vol. 16, no. 7, pp. 1670–1672, Jul. 2004.
[8] H. L. Chen, S. G. Li, Z. K. Fan, G. W. An, J. S. Li, and Y. Han, "A novel polarization splitter based on dual-core photonic crystal fiber with a liquid crystal modulation core," *IEEE Photon. J*., vol. 6, no. 4, pp. 1–9, Aug. 2014.
[9] H. Jiang *et al*., "Polarization splitter based on dual-core photonic crystal fiber," *Opt. Exp*., vol. 22, pp. 30461–30466, 2014.
[10] J. Zi, S. Li, G. An, and Z. Fan, "Short-length polarization splitter based on dual-core photonic crystal fiber with hexagonal lattice," *Opt. Commun*., vol. 363, pp. 80–84, 2016.
[11] K. Saitoh, Y. Sato, and M. Koshiba, "Polarization splitter in three-core photonic crystal fibers," *Opt. Exp*., vol. 12, pp. 3940–3946, 2004.
[12] H. E. Horng, C.-Y. Hong, S. Y. Yang, and H. C. Yang, "Designing the refractive indices by using magnetic fluids," *Appl. Phys. Lett*., vol. 82, pp. 2434–2436, 2003.
[13] L. Martinez, F. Cecelja, and R. Rakowski, "A novel magneto-optic ferrofluid material for sensor applications," *Sens. Actuators A, Phys*., vol. 123–124, pp. 438–443, 2005.
[14] Z. Peng *et al*., "Temperature-insensitive magnetic field sensor based on nanoparticle magnetic fluid and photonic crystal fiber," *IEEE Photon. J*., vol. 4, no. 2, pp. 491–498, Apr. 2012.
[15] W. Lin *et al*., "Magnetically controllable wavelength-division-multiplexing fiber coupler," *Opt. Exp*., vol. 23, pp. 11123–11134, May 2015.
[16] Y. Zhao, D. Wu, and R. Q. Lv, "Magnetic field sensor based on photonic crystal fiber taper coated with ferrofluid," *IEEE Photon. Technol. Lett*., vol. 27, no. 1, pp. 26–29, Jan. 2015.
[17] H. E. Horng, J. J. Chieh, Y. H. Chao, S. Y. Yang, C.-Y. Hong, and H. C. Yang, "Designing optical-fiber modulators by using magnetic fluids," *Opt. Lett*., vol. 30, pp. 543–545, 2005.
[18] G. P. Agrawal, *Nonlinear Fiber Optics*. New York, NY, USA: Academic, 2007.

[19] Y. F. Chen, S. Y. Yang, W. S. Tse, H. E. Horng, C.-Y. Hong, and H. C. Yang, "Thermal effect on the field-dependent refractive index of the magnetic fluid film," *Appl. Phys. Lett.*, vol. 82, pp. 3481–3483, 2003.
[20] C.-Y. Hong, S. Y. Yang, H. E. Horng, and H. C. Yang, "Control parameters for the tunable refractive index of magnetic fluid films," *J. Appl. Phys.*, vol. 94, pp. 3849–3852, 2003.